

## New trends in neutron imaging

Nikolay Kardjilov<sup>1\*</sup>, André Hilger<sup>1</sup>, Ingo Manke<sup>1,2</sup>, Markus Strobl<sup>1,3</sup>, Martin Dawson<sup>1</sup>, John Banhart<sup>1,2</sup>

<sup>1</sup> Helmholtz Centre Berlin for Materials and Energy, 14109 Berlin, Germany

<sup>2</sup> Berlin Institute of Technology, 10623 Berlin, Germany

<sup>3</sup> Ruprecht Karls University Heidelberg, 69120 Heidelberg, Germany

Neutron imaging is a method for non-destructive investigations of objects in science and engineering. Different contrast mechanisms provide information about the interior structure of samples. High-resolution neutron tomography is used for the reconstruction of the three-dimensional matrix of attenuation coefficients in the sample. Energy-selective radiography performed around Bragg-cut-off wavelengths makes structure defects and textures visible. Imaging with polarized neutrons makes it possible to visualize magnetic fields in bulk samples. Examples of different experimental techniques will be presented and discussed.

### 1. Introduction

The conventional neutron imaging technique is based on the mapping of the attenuation function for a neutron beam transmitting a sample. The obtained intensity map can be represented as an image with two main parameters – spatial resolution and contrast. The spatial resolution is influenced by the beam definition (collimation) and the detector system. The obtained contrast is governed by the interaction of the neutrons with matter. In conventional neutron radiography the contrast is given by beam attenuation through absorption and scattering in the sample. Using monochromatic neutrons for imaging one can get complimentary contrast due to the coherent scattering in polycrystalline materials. This allows one to perform Bragg-edge radiography which provides information about structural changes or composition inhomogeneities [1]. The neutron possesses a magnetic moment which makes it sensitive to magnetic fields. This kind of interaction can be used for two- and three-dimensional visualization of magnetic field distributions in free space and in bulk materials [2].

The mentioned contrast techniques require cold neutrons and a low background of high-energy gammas and fast neutrons due to the low intensity of the monochromatic beam used. These conditions are fulfilled at the neutron imaging beam line CONRAD at HZB [3]. The instrument is situated at a curved neutron guide, which filters out the majority of undesired gammas and fast neutrons providing a cold spectrum between 2 Å and 10 Å with a maximum at 3 Å. The special features of the instrument

were used to test different contrast techniques and detector improvements - a current trend in neutron imaging.

### 2. High resolution detector system

A limiting factor for the spatial resolution in imaging experiments is the detector system. Recently two different micro-set-ups with a field-of-view of about 25-30 mm and a resolution better than 50 µm have been realized [4,5]. The disadvantage of these set-ups is the high-cost of the detector systems. A conventional low-cost upgrade of the standard CCD based detector systems can provide comparable results. The use of a commercially available high-resolution lens system optimized for high-end digital cameras provides a 1:1 projection ratio without big losses of light intensity and image distortions. In this way the limiting factor is the pixel size of the CCD camera. Improvement of the scintillator screen can increase the resolution further. Using a cold neutron beam with a negligible gamma content is a precondition for applying scintillator screens based on Gadox (Gd<sub>2</sub>O<sub>2</sub>S(Tb)) active layers. The scintillating layer can be very thin in comparison to the standard <sup>6</sup>LiF based scintillators due to the higher cross-section of Gd for cold neutrons. Fig. 1a presents the result of a resolution test of a CCD-camera-based detector system using a 10 µm Gadox screen, 200 mm Nikon lens (AF Micro-Nikkor 200 mm f/4D) and 2048x2048 pixel CCD camera (Andor DW436N-BV).

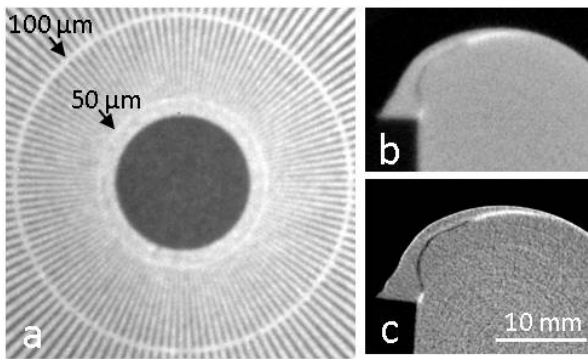


Fig. 1. a) Resolution test of a detector system based on 2048x2048 pixel CCD camera with 10  $\mu\text{m}$  Gadax scintillator screen using a standard Gd test pattern [6]; b) tomographic slice of a stainless steel piece with a crack using 200  $\mu\text{m}$   $^6\text{LiFZnS:Ag}$  screen and c) 10  $\mu\text{m}$  Gadax for the measurement.

The pixel size for the presented image was 13.5  $\mu\text{m}$  resulting in a field of view of 28 x 28  $\text{mm}^2$ . The achieved spatial resolution as seen in Fig. 1a was 50  $\mu\text{m}$ . The effect of the scintillator screen on the achieved resolution was studied by performing a tomographic investigation on a stainless steel piece with a standard 200  $\mu\text{m}$   $^6\text{LiFZnS:Ag}$  screen, Fig. 1b, and 10  $\mu\text{m}$  Gadax scintillator, Fig. 1c. The improvement of the resolution can be seen clearly in Fig. 1c where the 80  $\mu\text{m}$  crack and the remains of a contrast agent therein are resolved in detail.

## 2. Bragg-edge radiography

The neutron attenuation coefficient for polycrystalline materials decreases suddenly for well-defined neutron wavelengths – the so-called Bragg edges [7]. The position of these edges is defined by the symmetry and the parameters of the crystal lattice. At wavelengths greater than this critical value no scattering by particular  $\{h\ k\ l\}$  lattice spacings can occur because the corresponding Bragg reflection angle reaches its maximum of  $2\theta=180^\circ$ . Therefore a sharp increase in the transmitted intensity occurs.

Quantitative measurements around Bragg cut-offs for Fe and Al were performed with monochromatic neutrons by using the double crystal monochromator (PGC crystals with  $0.8^\circ$  mosaicity) [8] at the CONRAD instrument at HZB, and the data were compared with tabulated values [9]. Fig.2 shows the obtained results. The deviation from the tabulated values can be explained by texture orientations in polycrystalline materials [10].

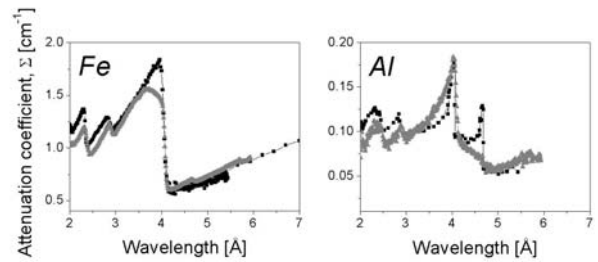


Fig. 2 Tabulated (dark,  $\blacksquare$ ) and radiographically (light,  $\blacktriangle$ ) measured attenuation coefficients of Fe and Al. The measurements were performed by double crystal monochromator with PGC- crystals having mosaicity of  $0.8^\circ$ .

The imaging technique with monochromatic neutrons can be used to tune the contrast in radiographs. Around the Bragg-cut-offs for a given material two different wavelengths can be found that have similar attenuation coefficients. The division of images taken at these wavelengths will cancel the contrast for that particular material. This will even work in tomographic investigations [1].

The position of the Bragg-cut-offs can be related to the correspondent  $d_{hkl}$  spacing. If areas of the sample have compressive or tensile residual stresses it will be reflected by a shift of the Bragg-cut-off position. On the other hand the height of the Bragg-cut-off is reciprocal to the number of crystallites having a defined orientation, which means that information about the distribution of texture fields in the sample can be extracted by studying the shape of the Bragg-cut-off [11,12].

In order to test this method, an Aluminium Foam Sandwich (AFS) precursor material of 10 mm thickness has been measured radiographically with a white beam (Fig. 3, left) and at a wavelength of 4.6  $\text{\AA}$  – close to the Bragg cut off for aluminium.

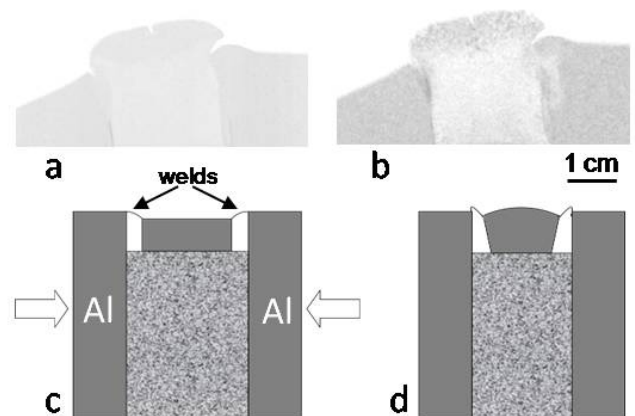


Fig. 3 AFS material visualised by a) a white neutron beam and b) a monochromatic beam at 4.6  $\text{\AA}$ . The container filled with aluminium foam c) is pressed uni-axially and later rolled to form the sandwich structure d).

The white beam image shows an average attenuation through the aluminium plates following the Beer-Lamberts law:  $I/I_0 = \exp(-\mu d)$ , where  $I_0$  is the primary beam intensity,  $I$  is the beam intensity after the sample transmission,  $d$  is the material thickness and  $\mu$  is the linear attenuation coefficient averaged over the whole neutron spectrum. The lack of contrast in Fig. 3a is due to the uniform thickness of sample and the homogeneous material composition. The image at a defined neutron wavelength shows contrast due to the coherent Bragg scattering. The dark areas in Fig. 3 b can be related to crystallites having the same orientation to the incident beam. Their formation can be explained by the manufacturing process illustrated in Fig. 3 c, d. An aluminium container consisting of welded plates is filled with Al foam precursor, Fig. 3 c. After the foaming the container is pressed uni-axially and a sandwich structure is produced by rolling as shown in Fig. 3 d. Due to the high temperature at welding and high pressure at rolling a recrystallization in the aluminium plates is possible.

#### 4. Spin polarized neutron imaging

Imaging methods with neutrons have the advantage that neutrons are able to pass through thick layers of matter (typically several centimeters). On the other hand the neutrons are sensitive to magnetic fields due to their magnetic moment, i.e. spin. Therefore as well as the conventional attenuation contrast image of a sample the magnetic field inside and around the sample can be visualized independently by detection of the polarization changes in the transmitted beam.

Polarized neutron radiography is based on the spatially resolved measurement of the final precession angles of a collimated and polarized monochromatic neutron beam that transmits a magnetic field, which is present inside and outside of a sample. Experiments using polarized neutrons were carried out at the neutron imaging beam line CONRAD at HZB [2]. For this purpose the instrument was equipped with solid state polarizing benders [13] providing a beam with a cross-section of 15 mm width and 45 mm height, Fig. 4. For larger samples a scanning arrangement was adopted for investigation of samples of up to 20 cm width. A double crystal monochromator device [8] was used to select a defined wavelength from the cold neutron spectrum. The achieved spatial resolution in the radiography images was around 500  $\mu\text{m}$  for the given experimental geometry.

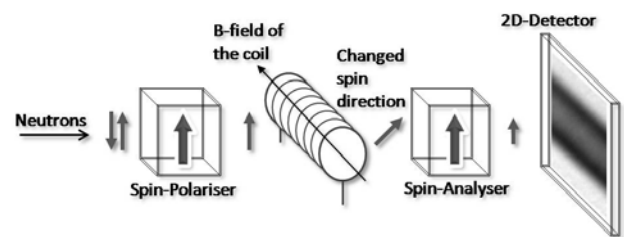


Fig. 4 Spin-polarized neutron imaging: The neutron spin rotates in the magnetic field of a sample and hence approaches the spin analyzer typically in a non-parallel orientation. The angle of the final spin rotation  $\varphi$  depends on the magnetic field integral along the beam path.

The potential of the method was demonstrated by the visualization of magnetic fields around a cylindrical coil at different current values, Fig. 5.

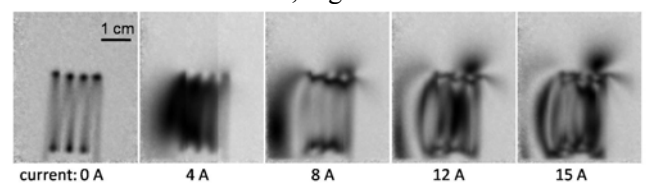


Fig. 5 Cylindrical coil investigated with polarized neutron radiography at different current values: The spin of the neutrons is rotated due to the coil's magnetic field which is perpendicular to the original spin orientation defined by the polarizer. The resultant spin orientation is converted by the transmission through the spin analyzer into gray levels between white for parallel and black for anti-parallel spin orientation with respect to the analyzer.

The spin polarized radiography can be used successfully for imaging the expelled and pinned magnetic field in superconductors [14,15]. An example of this is shown in Fig. 6

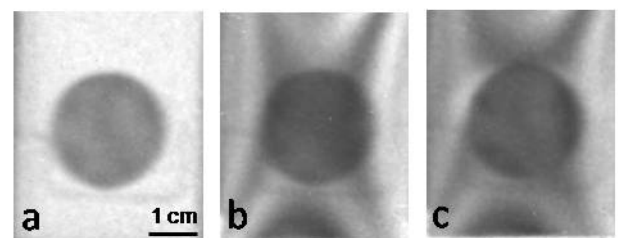


Fig. 6 Visualization of the Meissner effect by polarized neutron radiography: YBCO superconductor pellet (20 mm diameter, 5 mm thickness) at: a)  $T > T_c$ ,  $B = 0 \text{ mT}$ , b)  $T > T_c$ ,  $B = 2 \text{ mT}$ , c)  $T < T_c$ ,  $B = 2 \text{ mT}$ . The external magnetic field  $B$  is expelled from the sample volume at  $T < T_c$ . The critical temperature for YBCO ( $T_c$ ) is 94 K.

This new technique can be used to investigate many other physical effects of magnetism in the bulk of materials. In particular, the ability of neutrons to penetrate large volumes of many materials of up to several centimeters promises interesting applications in materials science.

## 5. Conclusions

The presented innovative techniques for neutron imaging use different contrast mechanisms to provide complimentary information to conventional absorption radiography and tomography. The further development of these techniques and their implementation as standard non-destructive methods requires beam lines and detector systems from a new generation with improved parameters (cold neutrons, low-background, high-resolution) and high flexibility.

## References

- [1] N. Kardjilov, S. Baechler, M. Basturk, M. Dierick, J. Jolie, E. Lehmann, T. Materna, B. Schillinger, P. Vontobel, Nucl. Instr. and Meth. A **501** (2003), S. 536-546
- [2] N. Kardjilov, I. Manke, M. Strobl, A. Hilger, W. Treimer, M. Meissner, T. Krist, J. Banhart, Nature Physics **4**, 399-403 (2008)
- [3] A. Hilger, N. Kardjilov, M. Strobl, W. Treimer, J. Banhart, Physica B **385-386** (2006), S. 1213-1215
- [4] E. H. Lehmann, G. Frei, G. Kühne, P. Boillat, Nucl. Instr. and Meth. A **576**, 389-396 (2007).
- [5] O. H.W. Siegmund, J. V. Vallerga, A. Martin, B. Feller, M. Arif, D. S. Hussey and D. L. Jacobson, Nucl. Instr. and Meth. A **579**, 188-191 (2007).
- [6] C. Grünzweig, G. Frei, E. Lehmann, G. Kühne, and C. David, Review of Scientific Instruments **78**, 053708 (2007).
- [7] S. Vogel, PhD. Thesis, available online at [http://eldiss.uni-kiel.de/macau/receive/dissertation\\_dis\\_00000330](http://eldiss.uni-kiel.de/macau/receive/dissertation_dis_00000330) (2000).
- [8] W. Treimer, M. Strobl, N. Kardjilov, A. Hilger, I. Manke, Applied Physics Letters **89**, 203504 (2006).
- [9] See for more details: <http://www-nds.iaea.org/exfor/exfor00.htm>
- [10] W. Kockelmann, G. Frei, E.H. Lehmann, P. Vontobel, J.R. Santisteban, Nucl. Instr. and Meth. A **578**, 421-434 (2007).
- [11] J. R. Santisteban, et al., J. Appl. Crystall. **34**, 289-297 (2001).
- [12] A. Steuwer, et al., Phys. Stat. Solidi (a) **185**, 221-230 (2001).
- [13] Th. Krist, S. J. Kennedy, T. J. Hick, F. Mezei, Physica B **241-243**, 82-85 (1998).
- [14] P. Gammel, D. Bishop, Science **279**, 410-411 (1998).
- [15] Ch. Jooss, J. Albrecht, H. Kuhn, S. Leonhardt, H. Kronmüller, Reports on Progress in Physics **65**, 651-788 (2002).